

Reconstructing the Arches I: Constraining the Initial Conditions

S. Harfst^{1*} and S. Portegies Zwart¹ and A. Stolte²

¹*Sterrewacht Leiden University, PO Box 9513, 2300 RA Leiden, The Netherlands*

²*1. Physikalisches Institut, University Cologne, Zùlpicher Str. 77, 50937 Köln, Germany*

31 May 2019

ABSTRACT

We have performed a series of N -body simulations to model the Arches cluster. Our aim is to find the best fitting model for the Arches cluster by comparing our simulations with observational data and to constrain the parameters for the initial conditions of the cluster. By neglecting the Galactic potential and stellar evolution, we are able to efficiently search through a large parameter space to determine e.g. the IMF, size, and mass of the cluster. We find, that the cluster’s observed present-day mass function can be well explained with an initial Salpeter IMF. The lower mass-limit of the IMF cannot be well constrained from our models. In our best models, the total mass and the virial radius of the cluster are initially $(5.1 \pm 0.8) \cdot 10^4 M_\odot$ and 0.76 ± 0.12 pc, respectively. The concentration parameter of the initial King model is $w_0 = 3 - 5$.

Key words: stars: formation – stellar dynamics – methods: N -body simulations

1 INTRODUCTION

The Arches cluster is one of only a few young and massive starburst clusters in the Milky Way. Its location at a projected distance of less than 30 pc from the Galactic center and an age of only ~ 2.5 Myr (Figer et al. 2002; Najarro et al. 2004) make this cluster a unique object for studying star formation and dynamical processes in the center of galaxies.

The observed present-day mass of the Arches cluster has been estimated with $\sim 1 - 2 \cdot 10^4 M_\odot$ (Figer et al. 1999; Espinoza et al. 2009). With this mass a cluster will not survive long in the Galactic center environment and evaporate on a time scale maybe as fast as ~ 10 Myr (Kim et al. 1999; Portegies Zwart et al. 2002). The initial mass of the cluster has been determined from N -body simulations, however, different results have been obtained by different authors: Kim et al. (2000) found that their best model for the Arches cluster had a total mass of about $2 \cdot 10^4 M_\odot$; Portegies Zwart et al. (2002), on the other hand, came to the conclusion that the cluster was initially more massive than $\sim 4 \cdot 10^4 M_\odot$.

The initial mass function (IMF), a key aspect of star formation, seems to be uniform throughout the universe (Kroupa 2002). This universal IMF can be described by the power-law found by Salpeter (1955) for stars in the solar neighborhood and is valid from $0.5 M_\odot$ to the highest

masses. Below $0.5 M_\odot$, the IMF is significantly flattened (e.g. Kroupa 2002).

Determining the IMF of young clusters from observations is not a straight-forward process. Uncertainties can arise from the measured luminosities, the estimated age of the cluster, the completeness of the observed sample, and the stellar evolution models. In addition, the non-linear dynamical evolution of the cluster has to be taken into account as shown in Fig. 1: as the star cluster evolves, more massive stars (star symbols) will move towards the cluster center and low-mass stars (points) in the opposite direction (indicated by the arrows in the left image). If the detection of cluster members is radially limited (dashed circle), it will result in an observed mass function (MF) in the mass-segregated cluster (right image) that is different from the IMF. This effect is visualized in Fig. 1 by the ratio of low- to high-mass stars inside the dashes circles before and after mass segregation.

In case of the Arches cluster, observations have revealed that the slope of the observed mass function (MF) is significantly flattened with $\Gamma \approx -0.9 \pm 0.15$ with respect to the standard Salpeter IMF ($\Gamma = -1.35$) (Stolte et al. 2005, 2002; Figer et al. 1999), and therefore the Arches cluster has been regarded as an argument against the universality of the IMF. More recently, however, Espinoza et al. (2009) derived a slope of $\Gamma = -1.1 \pm 0.2$ in $R < 0.4$ pc and concluded that a standard Salpeter IMF cannot be ruled out for Arches. In addition to the radial variation in A_V , these authors also accounted for differential extinction variations, which can

* harfst@strw.leidenuniv.nl

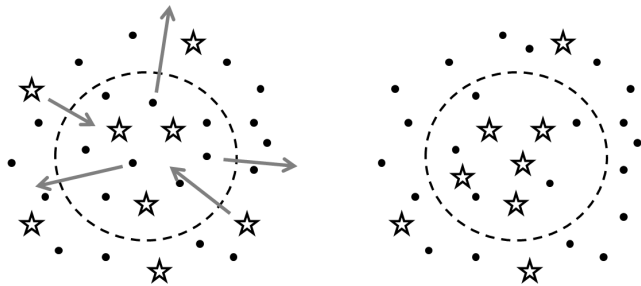


Figure 1. Schematic view on the cluster mass function and evolution. Low- and high-mass stars are shown by points and star symbols, respectively. The dashed circle indicates an radial observational limit. In the left image, the cluster is at $t = 0$ with arrows denoting the effects of dynamical evolution. The right image shows the mass-segregated cluster.

severely affect the incompleteness and may have biased the earlier results. Large uncertainties in the slope still remain, revealing the necessity to compare the observed cluster MF with simulations.

In addition to the flattened slope, there has been some debate whether the IMF of Arches is truncated at the low-mass end as the result of the extreme conditions at the Galactic center where the cluster has formed. Possible evidence for this was reported by Stolte et al. (2005), who determined a low- and intermediate-mass depleted MF in the cluster core ($R < 0.2$ pc) with a turn-over at $6 - 7 M_{\odot}$. This truncation in the MF was not seen by Kim et al. (2006). They only found a local bump in the MF at $\sim 6 M_{\odot}$. Even if the MF is truncated at the low-mass end, it remains unclear whether this would be the result of a truncated IMF or a dynamical effect such as tidal stripping of low-mass stars.

Several studies have been done to determine the IMF of the Arches cluster using numerical simulations, again coming to different conclusions: the model favored by Kim et al. (2000) started with flat IMF with a slope of $\Gamma = -0.75$ close to the observed one. Portegies Zwart et al. (2002) found that the observed IMF is the result of observational selection effects and dynamical evolution of the cluster. They argue that the observed flat MF is therefore consistent with a normal Salpeter IMF. And Kim et al. (2006) suggested that the initial slope of the MF was -1 to -1.1 , only slightly shallower than Salpeter.

The Arches cluster also exhibits clear signs of mass segregation. The slope of the observed MF for stars in different annuli changes with distance from the cluster center. Towards the center, the slope becomes shallower and further out the slope is closer to Salpeter (Kim et al. 2006; Stolte et al. 2005; Espinoza et al. 2009). Portegies Zwart et al. (2007) have found the same characteristics in numerical N -body models and concluded that the Arches cluster is about half-way to core collapse.

Despite the wealth of detailed observational data, large uncertainties regarding some of the properties of the Arches cluster remain, most importantly in the slope of the observed MF. Numerical simulations have been used to better understand the observations, but no fiducial model has emerged from these studies so far. In this paper, we want to reconstruct the initial properties of the Arches cluster by comparing the results of N -body simulations with observations.

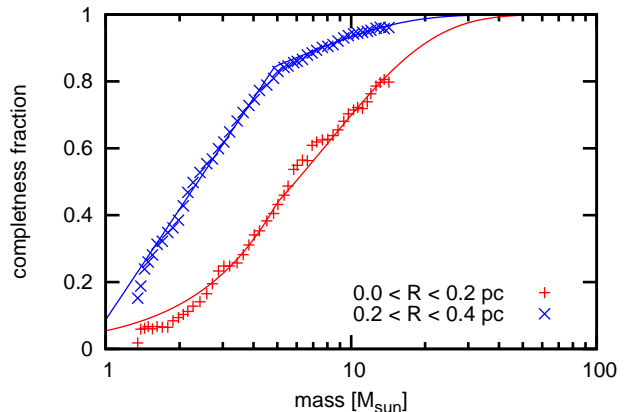


Figure 2. The completeness fraction in two radial bins as function of initial stellar mass. The data points (blue crosses and red pluses) are from the analysis of Stolte et al. (2005). The two full lines show a fit to the data.

In our N -body simulations, we model the Arches cluster on a star-by-star basis and, for the first time, systematically explore the parameter space to find the best set of initial conditions describing the Arches cluster. We vary parameters determining the initial mass, size, and concentration of the cluster. In addition, we also test which IMF can best explain the MF observed today. The total number of free parameters in our models is five, and a large number of simulations is required to search the full parameter space. Therefore, we decided to neglect the Galactic potential and stellar evolution for now. Once the initial conditions of the cluster have been constrained, we will use these results for simulation that include these processes in a follow-up paper.

The paper is outlined as follows: in Sec. 2, we describe the observational data we use. Then we explain the parameters for the cluster model in Sec. 3 and the simulations and their results in Sec. 4. We conclude and summarize in Sec. 5 and Sec. 6.

2 OBSERVATIONAL DATA

We use data from observations by Stolte et al. (2005, NACO data hereafter). The NACO data has been taken using the ESO VLT AO system NAOS and the CONICA near-infrared camera in two wave bands, H and K_s . The field of view is $\sim 25''$ squared or 1 pc^2 (we assume a distance of 8 kpc to the cluster) with a resolution of $\sim 0.''08$.

The total data set consists of ~ 2200 stars belonging to the cluster and the field. In order to find the cluster stars, we apply the same colour selection as Stolte et al. (2005) (see their Fig. 2), leaving ~ 1500 stars. We then fit the K -band magnitudes (corrected for the observed radial variation in extinction (Stolte et al. 2002)) against a 2.5 Myr Geneva main-sequence isochrone (Lejeune & Schaerer 2001), assuming solar metallicity for Arches (Najarro et al. 2004). From this we get both present-day and initial stellar masses for each star in the sample.

Because the incompleteness of the data due to crowding effects increases significantly for stars towards the low-mass end we reduced the sample further to about 300 stars by

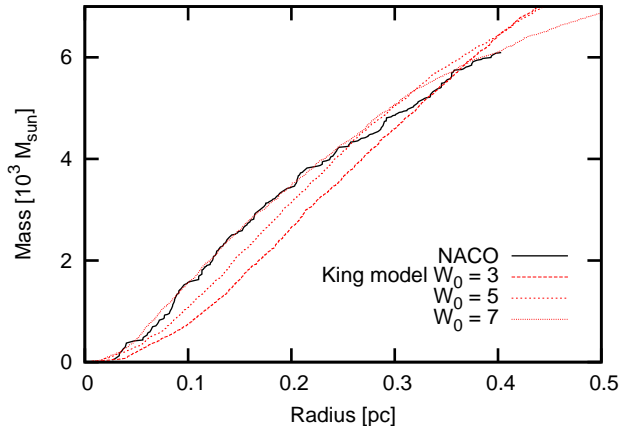


Figure 3. The cumulative mass profile for stars with $m > 10 M_{\odot}$.

selecting only massive stars with $m > 10 M_{\odot}$. With our chosen lower mass limit, the data is 80% complete or better for any star mass and position, as a detailed analysis by Stolte et al. (2005) has shown. Fig. 2 shows the completeness fraction as a function of initial stellar mass for two different radial bins. We have fitted the results of Stolte et al. (2005, blue crosses and red pluses in Fig. 2) and also extrapolated for stellar masses above $\sim 15 M_{\odot}$. In the following analysis, we use this information to either correct the observational data or by randomly removing stars from our models. Note that only a few stars are added or removed by this correction for $m > 10 M_{\odot}$.

The field-of-view of the NACO data is such that only within a limited radius all stars of the cluster can be seen. This radius is 0.4 pc (see left panel in Fig. 11 which shows an image of all the ~ 1500 cluster stars; the radius of 0.4 pc is indicated by a circle centered on the center of density). We therefore also limit our sample to the 234 massive stars within this radius. The cumulative mass profile for these stars is shown in Fig. 3, where we also show the mass profiles for three different King models (King 1966). All models have the same virial radius $r_{\text{vir}} = 0.5$ pc and are scaled in mass to approximately fit the observed profile. The present-day profile of the Arches cluster is best described by a King model with $W_0 = 7$.

3 THE MODEL OF THE ARCHES CLUSTER

In order to construct a model for the Arches cluster, we compare the results of N -body simulations with the observational data described above. The simulations start from a set of initial conditions with a number of parameters that can be varied to find the best fitting model. We have chosen the IMF, total mass, concentration, and size of the cluster as the free parameters. Other parameters are fixed: we assume an age of 2.5 Myr and a distance of 8 kpc to the cluster.

3.1 Initial Mass Function

It has been discussed whether the IMF of the Arches cluster deviates from the norm, with a flattened distribution (for massive stars) with respect to a Salpeter IMF. Determining

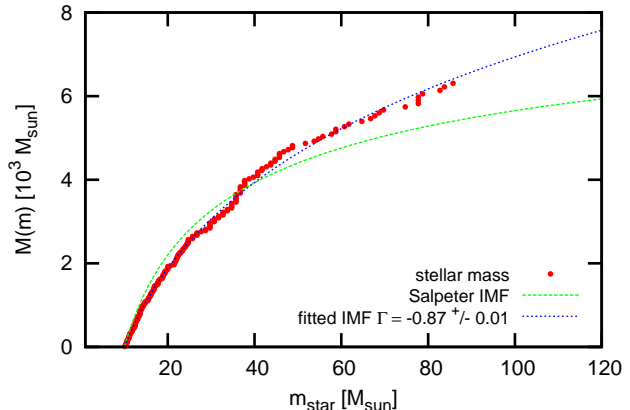


Figure 4. The cumulative observed MF of massive stars ($m > 10 M_{\odot}$) in the Arches cluster (red dots). The dotted blue line is a fitted power-law MF and the green dashed line is a Salpeter MF. Data is from Stolte et al. (2005) and corrected for incompleteness.

the IMF of a star cluster is not a straight-forward process. The present-day mass function (PDMF) of a cluster is the result of stellar evolution and dynamical effects. In addition, selection effects then shape the observed MF, which will use in the following for the comparison with our models. We do not take into account stellar evolution, and we use the initial masses of stars to determine the observed mass function (using the present-day masses of stars would change the MF only for stars with $m > 50 M_{\odot}$). We also correct the observed MF for the incompleteness of the data, however, the observed MF can differ from the underlying IMF due to the selection of stars inside $R < 0.4$ pc

We derive the observed MF from the NACO data and also find a shallow slope with $\Gamma = -0.9 \pm 0.15$ for stars with $m > 10 M_{\odot}$ in Fig. 4. We correct for the incompleteness of the data by weighting stellar masses with the inverse of the completeness fraction given in Fig. 2. The slope is derived by fitting an integrated power-law MF with two free parameters (normalization and slope) to the cumulative observed MF. This allows a more straight-forward fitting of the data than the commonly used mass binning. The formal uncertainty of the fit is small (see Fig. 4) and not taking into account errors in determining stellar masses. Stolte (2003) has given an estimate of ± 0.15 for the total error, which we also use here.

The slope we find here is in agreement with what has been reported by Stolte et al. (2005), and significantly deviates from a standard Salpeter MF. As a test, we have created random realizations of the Salpeter MF using $1 M_{\odot}$ and $120 M_{\odot}$ as the lower and upper mass limit, respectively. The total number of models was 1000 and each model consisted of 7500 stars which, on average, results in 250 stars with $m > 10 M_{\odot}$. We then fitted a power-law MF to each of the models in the same way we fitted the observed MF, using only the ~ 250 massive stars. In Fig. 5, we show the distribution of fitted Γ -values and from this distribution we derive $\Gamma = -1.34 \pm 0.12$. The Γ -value derived from the observations is indicated by the shaded box. Based on this, only a small fraction of our models (nine) are consistent with the observed MF. However, given the uncertainties in deriving

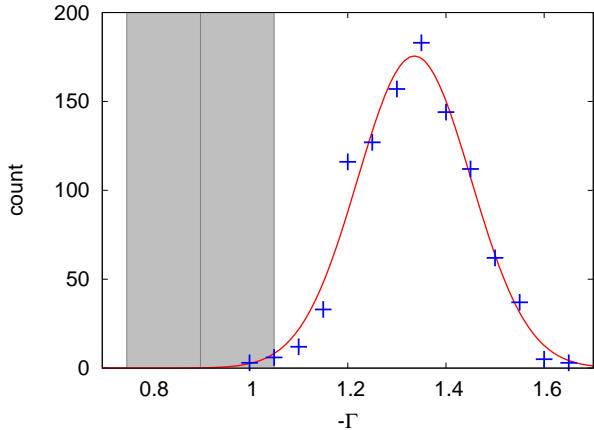


Figure 5. The distribution of fitted Γ -values of model MFs. Shown are the results from the models (blue pluses) together with a fitted Gaussian distribution. The observed MF slope is indicated by the shaded area.

the initial masses of stars (which depend very much on the model for the rather unknown mass loss rate) and since so far any effects from the dynamical evolution of the cluster are not taken into account, we decided to use the slope of the IMF as a free parameter and studied, how a different IMF affects the present-day MF in the dynamically evolved and mass-segregated cluster. We also varied the lower mass limit of the IMF to test for a possible truncation of the IMF at lower masses.

3.2 Initial mass of the cluster

The choice of an IMF is also important for determining the total mass of the cluster. The present day mass of the cluster is $\sim 1 - 2 \cdot 10^4 M_\odot$ (Figer et al. 2002; Stolte et al. 2008; Espinoza et al. 2009). Kim et al. (2000) estimate that Arches could have lost about half its initial mass due to its dynamical evolution in the Galactic center, which would give an initial mass of $\sim 3 \cdot 10^4 M_\odot$. On the other hand, Figer et al. (2002) calculated an upper mass limit of $7 \cdot 10^4 M_\odot$ for the cluster, based on the virial theorem and the observed velocity dispersion.

In Fig. 6, we show the initial cluster mass we derive for different IMFs. For each IMF we used three different normalizations such that the total number N_{MS} of star more massive than $20 M_\odot$ is 200, 250, and 300. We then varied the lower mass limit of the IMF as it may be truncated in the Arches cluster (Stolte et al. 2005).

We find, that the total cluster mass can be initially as high as $\sim 8 \cdot 10^4 M_\odot$ (Salpeter IMF) or even higher if stars below $0.5 M_\odot$ have formed in the cluster. For a flat IMF ($\Gamma = -0.9$), the total cluster mass does not depend much on the lower cut-off and is for $N_{\text{MS}} = 200$ about $\sim 2 \cdot 10^4 M_\odot$ in good agreement with the findings of Kim et al. (2000).

3.3 Size of the cluster

The Arches is a very dense cluster with a central mass density of $\sim 2 \cdot 10^5 M_\odot \text{pc}^{-3}$ (Espinoza et al. 2009). The tidal radius of the Arches cluster is $\sim 1 \text{pc}$ and we determine

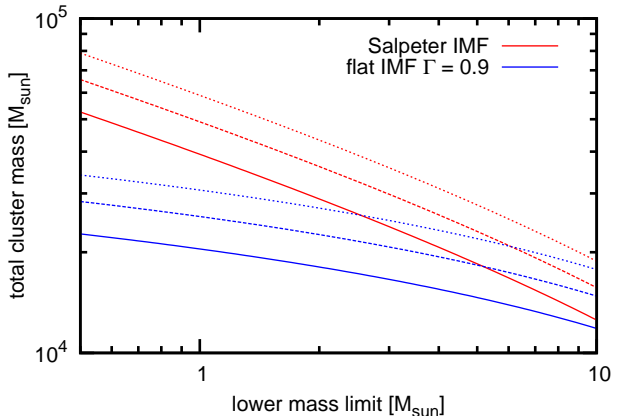


Figure 6. The initial mass of the cluster as a function of the lower mass-limit of the IMF for different IMFs. The three lines show different normalizations.

the core radius with $r_{\text{core}} = 0.25 \text{pc}$ using all stars and with $r_{\text{core}} = 0.14 \text{pc}$ for stars with $m > 10 M_\odot$. Following Casertano & Hut (1985), the core radius is defined throughout this paper as the density-weighted average distance of stars to the density center.

The current concentration of the Arches cluster may be the result of its dynamical evolution as the cluster is probably evolving towards core collapse. We therefore use the initial concentration, parameterized in the King model concentration parameter w_0 , and size of the cluster, namely its virial radius, as two more free parameter. The virial radius r_{vir} is defined as

$$r_{\text{vir}} = \frac{1}{2} \frac{GM^2}{|U|} \quad (1)$$

with the gravitational constant G , the mass M and potential energy U of the cluster. Since U cannot be observed, it may be more practical to know that the virial radius is proportional to the half mass radius.

3.4 Summary of model parameters

To summarize, the initial conditions for our cluster models are set by the virial radius, slope and low-mass cutoff of the IMF, concentration, and number of massive stars, which are varied systematically (see Tab. 1 below and Sec. 4.1).

4 SETUP AND RESULTS OF SIMULATIONS

Our aim is to find a numerical model of the Arches cluster that can explain the observed properties of the cluster. In this paper, we neglect the effects of the Galactic potential as well as stellar evolution. This allows us to perform a large number of simulations in order to constrain some of the parameters of our models. The simulations were carried out in the **Starlab** environment using the integrator **kira** (Portegies Zwart et al. 2001). GPUs, graphical processing units, were used to accelerate the calculations via the **Sapporo** library (Gaburov et al. 2009).

Table 1. List of models.

Model	W_0	IMF	m_{low}	M_{cluster}	N_{cluster}	$N(m > 10 M_{\odot})$	parameter	
							$R_{\text{vir}}[\text{pc}]$	N_{MS}
IKW03F05	3	flat	0.5	22.9	6.9	423	0.1 – 1.0	100 – 300
IKW03F10	3	flat	1.0	20.5	3.7	421	0.1 – 1.0	100 – 300
IKW03S05	3	Salpeter	0.5	52.7	31.9	552	0.1 – 1.0	100 – 300
IKW03S10	3	Salpeter	1.0	39.7	12.5	552	0.1 – 1.0	100 – 300
IKW03S40	3	Salpeter	4.0	20.6	1.9	540	0.1 – 1.0	100 – 300
IKW05F05	5	flat	0.5	22.7	6.9	413	0.1 – 1.0	100 – 300
IKW05F10	5	flat	1.0	20.2	3.7	413	0.1 – 1.0	100 – 300
IKW05S10	5	Salpeter	1.0	39.0	12.5	545	0.1 – 1.0	100 – 300
IKW05S40	5	Salpeter	4.0	20.8	1.9	543	0.1 – 1.0	100 – 300
IKW07F05	7	flat	0.5	22.9	6.9	422	0.1 – 1.0	100 – 300
IKW07F10	7	flat	1.0	20.7	3.7	421	0.1 – 1.0	100 – 300
IKW07S10	7	Salpeter	1.0	39.2	12.5	537	0.1 – 1.0	100 – 300
IKW07S40	7	Salpeter	4.0	20.8	1.9	551	0.1 – 1.0	100 – 300

Columns are: 1) model name; 2) the dimensionless King concentration parameter W_0 3) the IMF used, where flat and Salpeter refer to power-law IMFs with $\Gamma = -0.9$ and $\Gamma = -1.35$, respectively; 4) lower IMF mass limit in M_{\odot} ; 5) total cluster mass in $10^3 M_{\odot}$; 6) total number of stars in the cluster in 10^3 ; 7) total number of massive stars ($m > 10 M_{\odot}$); 8) additional model parameter and range

4.1 Initial conditions

We use King models (King 1966) in virial equilibrium as our initial cluster model. As the initial concentration of the cluster is not known, it is possible that the cluster has evolved to its current compactness from a less concentrated model. We therefore decided to use three different values for the initial concentration parameter W_0 . For each concentration parameter we also tested both the Salpeter IMF and an IMF with a flat slope of $\Gamma = -0.9$. Furthermore, we also varied the lower mass limit of the IMF between $0.5 M_{\odot}$ and $4 M_{\odot}$. In total, we used 13 different sets of initial conditions for the cluster (see Tab. 1).

In addition, we also varied two free parameters for each of these models: the initial virial radius as r_{vir} and the initial number N_{MS} of stars with $m > 20 M_{\odot}$. The latter is used to normalize the total cluster mass and we used five different values for N_{MS} between 100 and 300 in steps of 50. This range covers the 127 stars with $m > 20 M_{\odot}$ found in the NACO data and the ~ 200 stars reported by Figer et al. (2002), also taking into account that a significant fraction of massive stars is no longer bound to the cluster or not observed. The differences between the two data sets can be explained by a different field-of-view (smaller for NACO) and the applied selection criteria to determine cluster membership. Varying N_{MS} increases the total number of models tested to 65.

Our N -body simulations are scale-free N -body units because we neglect stellar evolution and the tidal field. In N -body units, the gravitational constant G , the total mass of the system, and the virial radius are all set to unity (Heggie & Mathieu 1986). The connection between the scale-free N -body units and physical units is then given by

$$G = 1 \frac{U_1^3}{U_m U_t^2} = 0.0045 \frac{\text{pc}^3}{M_{\odot} \text{Myr}^2}, \quad (2)$$

where U_1 , U_m , and U_t are the N -body units for length, mass, and time, respectively. The mass unit U_m is naturally given by the total mass of the Arches cluster M_{Arches} . A choice of

r_{vir} defines U_1 , which in turn determines U_t via Eq. 2. The age of the cluster is $t = 2.5 \text{ Myr}$ or according to Eq. 2

$$t = \frac{2.5 \text{ Myr}}{U_t} = 2.5 \cdot \sqrt{0.0045 \frac{M_{\text{Arches}}}{M_{\odot}} \left(\frac{r_{\text{vir}}}{\text{pc}} \right)^{-3}} \quad (3)$$

in the dimensionless N -body time unit.

The virial radius was varied between 0.1 and 1 pc in steps of 0.05 pc. However, instead of increasing the number of models by another factor of 19, we make use of the scale-free nature of our simulations. For each value of r_{vir} , the cluster has to be evolved to a different N -body time unit given by Eq. 3 to reach an age of 2.5 Myr in physical units. The N -body times to match the desired values of r_{vir} can be computed at the start of the simulation, and then snapshots are written at these N -body times during this simulations. Each of the snapshots corresponds to a snapshot of the Arches cluster at $t = 2.5 \text{ Myr}$ with a different r_{vir} .

Each of the 65 models was created ten times with a different random realization, so that a total of 650 simulations were performed. However, once the simulations were finished, we averaged the global properties of each model before comparing them with the observations. We also took into account the incompleteness of the observations by randomly removing a few stars from our models according to the incompleteness tests by Stolte et al. (2005). However, this has only little effect on the overall results as we already constrained our data sample to stars that are almost complete in the observations. In the end, we compared more than 1,200 simulation snapshots with the observations.

4.2 Comparing models and observation

In order to compare the simulation snapshots with the NACO data, we first computed a cumulative mass profile for each parameter set. In this process, we averaged the ten different random realizations and obtained a single mass profile. We only selected stars with $m > 10 M_{\odot}$ and within $r < 0.4 \text{ pc}$ and we also normalized the profile to the total mass inside this radius. Two of the resulting profiles are

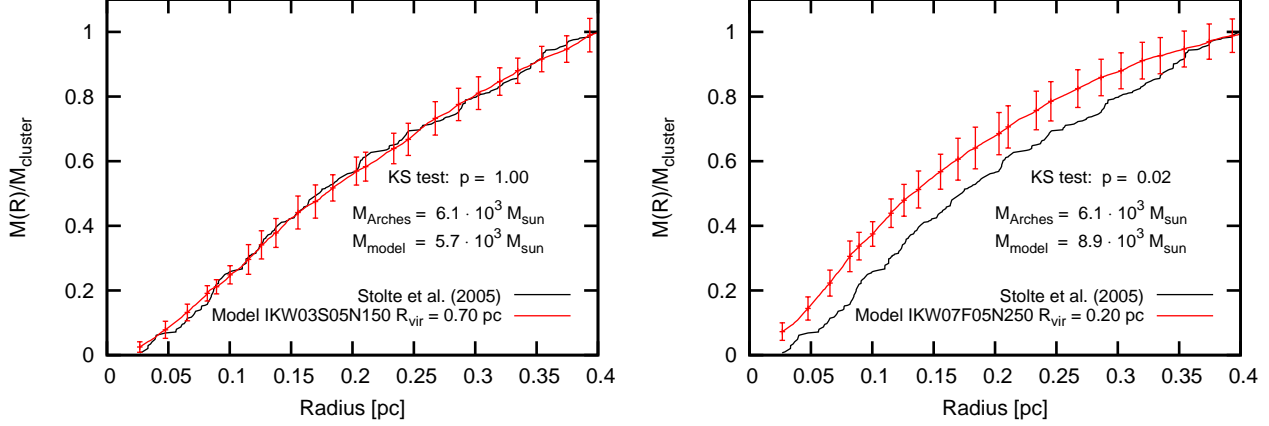


Figure 7. Comparing the normalized cumulative mass profile of model and observation. The red line shows the model data, with error bars indicating the standard deviation from averaging over ten random realization of the same model. The black line the observation. Two different models are shown.

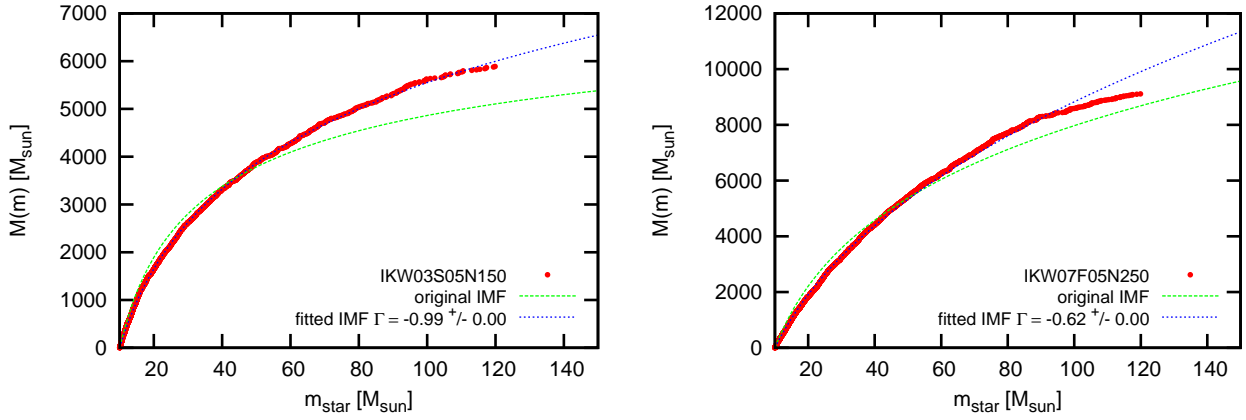


Figure 8. Comparing the cumulative mass function of model and observation. The red line shows the model data, with error bars indicating the standard deviation from averaging over ten random realization of the same model. The green line shows the original IMF that was used to setup the ICs for the model. Two different models are shown.

shown in Fig. 7 (red line with error bars) in comparison with the observed profile (black line).

In the following we define a number of fitness parameters f which describe the quality of the fit of the model to the observation. These parameters are defined such that the values range from zero to unity. A value close to unity describes a good fit.

The mass profile fitness parameter f_p is used to quantify how well the cumulative mass profile of the model fits the observations. We employ a two-sample KS test (see Press et al. 1992) for this comparison. The KS-test returns the probability p , that two data sets are drawn from the same distribution. In Fig. 7, the p -value is given for two different models and it can be seen that a good fit results in a high p -value as expected. In the following, we will use

$$f_p = p, \quad (4)$$

where a value of f_p close to unity describes an excellent fit.

We also compare the total mass of stars with $m > 10 M_\odot$ inside of 0.4 pc. We define the mass fitness param-

eter

$$f_M = 1 - \left| 1 - \frac{M_{\text{model}}}{M_{\text{Arches}}} \right| \quad (5)$$

as an estimator for how well the observed total mass of the cluster is reproduced in the model. $f_M = 1$ identifies a perfect match and becomes smaller the more M_{model} deviates from M_{Arches} .

In Fig. 8, we show the comparison of the observed cumulative MF for the Arches cluster with our models. The integrated MF of the model (red dots) is fitted by a power-law MF (dotted blue line) to determine the slope Γ . Two different models are shown, which started out with a Salpeter IMF (left panel) and a flat IMF (right panel). The IMF used for the initial conditions of the model is also plotted in each panel (dashed green line). Because we only take stars within 0.4 pc into account, the measured (observed) MF can differ significantly from the original IMF. Similar to f_M , we define the MF fitness parameter

$$f_{\text{IMF}} = 1 - \left| 1 - \frac{\Gamma_{\text{model}}}{\Gamma_{\text{Arches}}} \right| \quad (6)$$

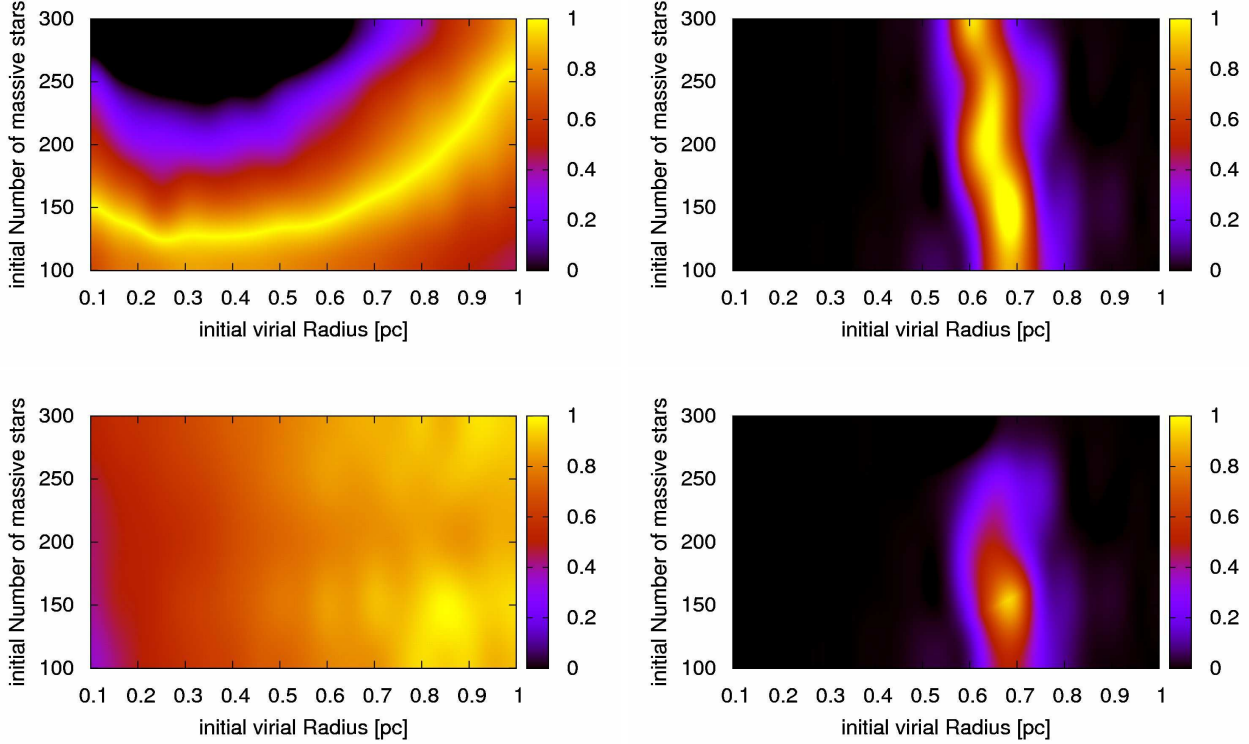


Figure 9. Quality of fit to observations for varying model parameters r_{vir} and N_{MS} . Data from model IKW03S10 (isolated King model with $W_0 = 3$ and a Salpeter IMF with $m_{\text{low}} = 0.5 M_{\odot}$). Panels show from top left to bottom right the fit to the cluster mass, cumulative mass profile, IMF and product of all three fits. A fitness parameter close or equal to unity indicates the best fit models.

with $\Gamma_{\text{Arches}} = -0.9$.

The quality of the fit for model IKW03S05 is presented in Fig. 9, which shows how f_p , f_M , and f_{IMF} vary for the model parameters r_{vir} and N_{MS} . The cluster mass is best fitted with $N_{\text{MS}} \approx 150$ and almost independent of r_{vir} . Only models with $r_{\text{vir}} \geq 0.8$ require larger values of N_{MS} . This can be explained as follows: models with small r_{vir} evolve faster dynamically and these models have gone through core collapse already at an age of 2.5 Myr. As a result, the initial dependence of N_{MS} on r_{vir} , which can still be seen for larger values of r_{vir} , is lost.

The top right panel in Fig. 9 shows which models have the best fitting mass profiles. In this case, the best models are found within a narrow range of r_{vir} -values with no dependence on N_{MS} . Models with $r_{\text{vir}} \leq 0.5$ pc are, in comparison with the observations, too concentrated (see also Fig. 7) whereas $r_{\text{vir}} > 0.8$ pc results in a too shallow mass profile.

The slope of the IMF depends not as strongly on the model parameters (bottom left panel) though the general trend is, that the best fits are found for larger values of r_{vir} . In the last panel, we show the combined fitness f_{all} which is defined as

$$f_{\text{all}} = f_p \cdot f_M \cdot f_{\text{IMF}}. \quad (7)$$

From this, we find the best fitting model in the model series IKW03S05, which has the virial radius $r_{\text{vir}} = 0.70$ pc and $N_{\text{MS}} = 150$. The number of stars with $m > 10 M_{\odot}$ and inside $R < 0.4$ pc in this particular model is 208 ± 12 (averaged over

ten random realizations), compared to 234 in the observed sample.

In Fig. 10 we compare f_{all} for a number of different model series. The two panels at the top show the results for the models IKW03S10 and IKW03S40. The only difference between these two models and also to model IKW03S05 shown in Fig. 9 is the lower mass limit of the IMF, which is 1.0 , 4.0 , and $0.5 M_{\odot}$, respectively. In each of the three models the best fit is in a similar regime of the parameter space, with $r_{\text{vir}} = 0.6 - 0.7$ pc and $N_{\text{MS}} \approx 150$. In the other four models shown, the best fitting models also lie within a small area of the parameter space.

The two bottom panels show results from models starting initially with a flat IMF. These models produce not as good a fit as models starting with a Salpeter IMF. The reason is that the slope of the IMF is always flattened by the dynamical evolution of the cluster (see also Fig. 8), so that models starting with the observed slope cannot produce a good fit. This result is independent of the initial concentration of the cluster though more concentrated clusters give slightly better results.

We have summarized the results in Tab. 2 where for each model series the best values for r_{vir} and N_{MS} are given together with the corresponding value of f_{all} . We also repeated the whole analysis using all stars down to $4 M_{\odot}$ in the comparison. In both cases, models with the highest values of f_{all} all have a Salpeter IMF. These best fit models also have similar value of r_{vir} and N_{MS} . We computed the average of these values weighted with f_{all} which results in

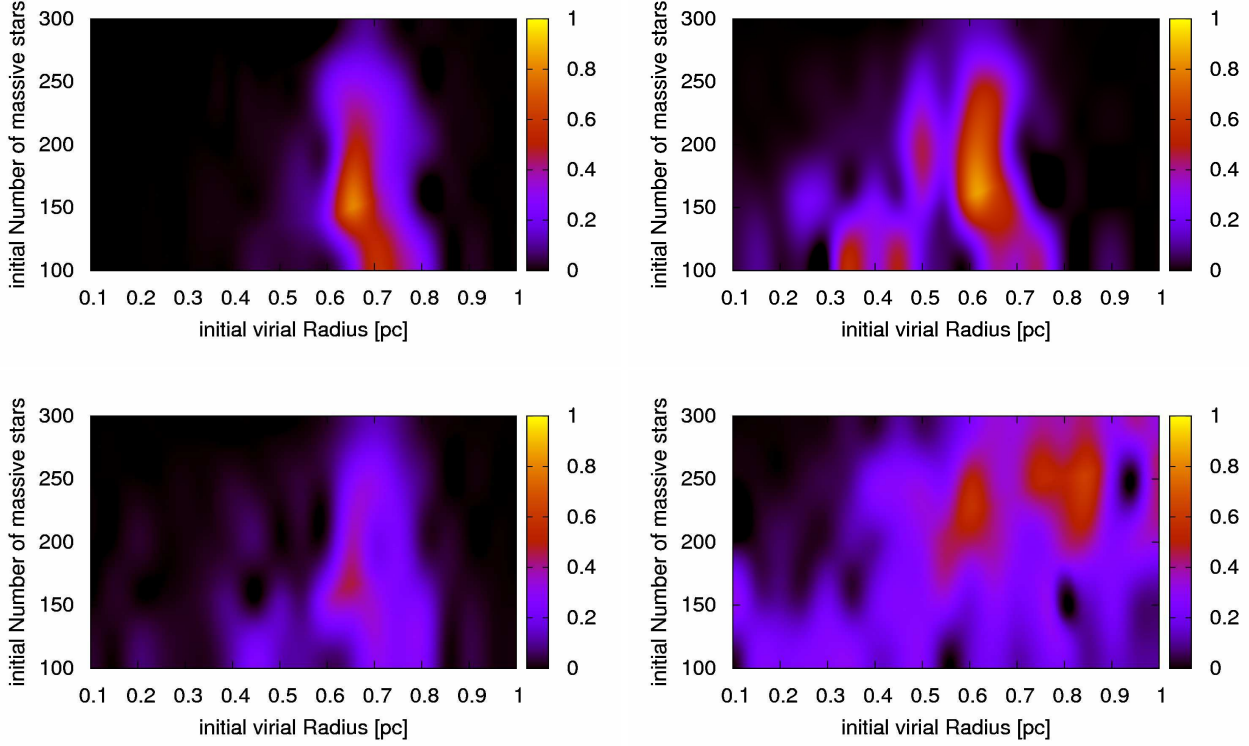


Figure 10. Quality of fit to observations for different models and varying model parameters r_{vir} and N_{MS} . The combined fitness f_{all} is shown for models IKW03S10, IKW03S40, IKW03F05, and IKW07F10 from top left to bottom right, respectively.

Table 2. Best fitting models.

Model	parameter		f_{all}	
	$R_{\text{vir}}[\text{pc}]$	N_{MS}	$m > 10 M_{\odot}$	$m > 4 M_{\odot}$
IKW03F05	0.65	200	0.37	0.45
IKW03F10	0.7	200	0.43	0.47
IKW03S05	0.7	150	0.85	0.68
IKW03S10	0.65	150	0.79	0.82
IKW03S40	0.6	200	0.66	0.56
IKW05F05	0.85	200	0.46	0.45
IKW05F10	0.9	250	0.48	0.42
IKW05S10	0.8	200	0.69	0.64
IKW05S40	0.75	200	0.88	0.77
IKW07F05	0.75	200	0.52	0.43
IKW07F10	0.85	250	0.62	0.41
IKW07S10	1.0	200	0.66	0.76
IKW07S40	0.85	250	0.78	0.70

Columns are: 1) model name; 2) values of additional model parameter; 3) and 4) f_{all} comparing stars with $m > 10 M_{\odot}$ and $m > 4 M_{\odot}$

$r_{\text{vir}} = 0.76 \pm 0.12 \text{ pc}$ and $N_{\text{MS}} = 192 \pm 32$ for the comparison using stars with $m > 10 M_{\odot}$ and $r_{\text{vir}} = 0.62 \pm 0.15 \text{ pc}$ and $N_{\text{MS}} = 164 \pm 35$ for stars with $m > 4 M_{\odot}$. The initial mass of the cluster depends on the lower mass limit of the IMF which is not constrained by our models unfortunately. Based on our results for stars with $m > 10 M_{\odot}$, we get $M = (51 \pm 8) \cdot 10^3 M_{\odot}$, $M = (38 \pm 6) \cdot 10^3 M_{\odot}$, and

$M = (20 \pm 3) \cdot 10^3 M_{\odot}$ for lower mass limits of the IMF of 0.5, 1, $4 M_{\odot}$.

5 DISCUSSION

A number of models in Tab. 2 can be considered best fit models, for example model IKW03S05 with $r_{\text{vir}} = 0.70$ and $N_{\text{MS}} = 150$. A snapshot of this model at $t = 2.5 \text{ Myr}$ is shown in Fig. 11. Stellar masses are indicated by the point size and gray-scale and the center of density of the cluster is located at the origin. The dashed circle has a radius of 0.4 pc. In the left panel, the NACO data is plotted for comparison in the same way as the simulation data in the right panel. In the latter, stars have been randomly removed to mimic incompleteness. The probability that a star is removed is given by a function fitted to the data shown in Fig. 2 and depends on mass and position of the star.

At 2.5 Myr, the cluster has a total mass of $\sim 2 \cdot 10^4 M_{\odot}$ inside a radius of 0.4 pc and twice that mass inside the tidal radius of 1 pc. On average, our best models predict that the Arches cluster is more massive than observed, even if we take into account mass loss by stellar evolution. About $6 \cdot 10^3 M_{\odot}$ of the total mass are in stars below $1 M_{\odot}$. Our results are in good agreement with the previous findings of Portegies Zwart et al. (2002).

Generally, only models with the Salpeter IMF produce acceptable fits and we therefore conclude that the IMF in the Arches cluster is normal despite the extreme environment in which the cluster is formed. However, we cannot rule out a turn-over as suggested by (Stolte et al. 2005) as our results

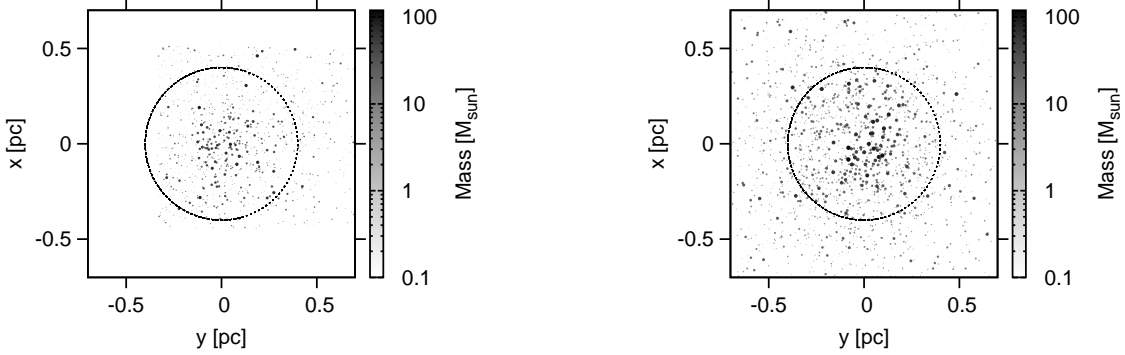


Figure 11. The observed cluster (left) and a snapshot of one of the best fitting models (right) in comparison. The images are centered on the center of density and the circles indicate a radius of 0.4 pc. Gray-scale and point size represent stellar masses. In the right panel, stars have been removed randomly to mimic incompleteness.

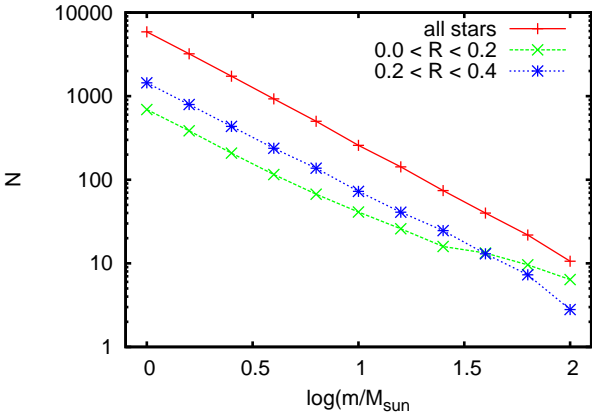


Figure 12. The IMF of the best fitting model for all stars and the stars in two radial bins.

are not very sensitive to the lower mass limit of the IMF. Our best fitting models can have any lower mass limit in the range of $0.5 - 4.0 M_{\odot}$ that we investigated.

Fig. 12 shows the MF of one of our best fit models. A bin size of $\Delta \log(m/M_{\odot}) = 0.2$ was used to obtain the individual star counts and the data was also averaged over the ten different realization of this model. The top line shows the MF for all stars which is simply the Salpeter IMF used in the initial conditions of this model. The other two lines show the MF in two radial bins (the same used by Stolte et al. (2005) and Espinoza et al. (2009)). The MF is noticeably flattened for massive stars ($m \gtrsim 10 M_{\odot}$) in the inner radial bin ($R < 0.2$ pc), while it remains unchanged in the outer radial bin ($0.2 < R < 0.4$ pc). The flattening of the MF in the cluster core has been reported in all the previous observational studies, though with varying Γ -values determined for the slope. Our best fit models are in very good agreement, however, with the latest results from Espinoza et al. (2009). Stars with $m > 10 M_{\odot}$ can be found in our models as far as 10 pc from the cluster center. However, we find that in order to measure the correct slope of the MF, we only need the stars inside the tidal radius of 1 pc.

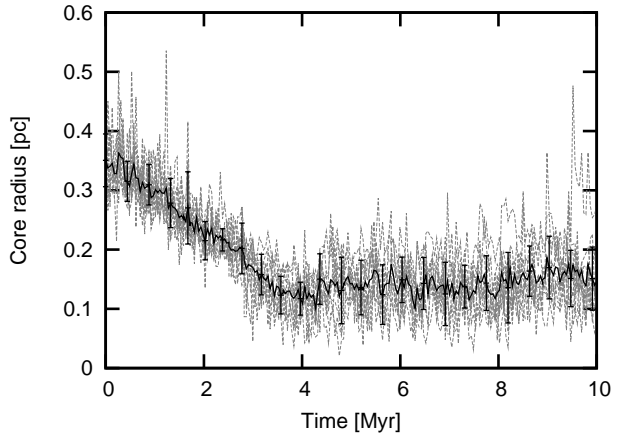


Figure 13. The core radius evolution with time of model IKW03S05 with $r_{\text{vir}} = 0.7$ pc and $N_{\text{MS}} = 150$. The black line with errorbars shows the average of ten random realizations of the same model (grey lines). Core collapse happens at ~ 4 Myr.

No turn-over at the low mass end of the IMF can be seen. This means that the turn-over seen by Stolte et al. (2005) cannot be explained by mass segregation (unlike the flat IMF at the high-mass end). Deriving the IMF from our simulation data is not hampered by incompleteness, selection effects, and mass determination from observed luminosities. All these effects may bias the observed star counts to produce a turn-over, however, the turn-over appears at $\sim 6 M_{\odot}$ where the data is still 50% complete. So, either the IMF is indeed truncated or another effect has to be considered. One possible explanation is that tidal stripping preferably removes low-mass stars from the cluster. This effect is not included in our current simulations but will be tested in a follow-up paper. Alternatively, Espinoza et al. (2009) pointed out that local variations in extinction can account for (some of) the flattening of the observed MF. The same effect could cause lower-mass stars to be lost preferentially. Then the completeness function, which only takes into account crowding and sensitivity effect, would not be sufficient to correct the low-mass end of the IMF.

In Fig. 13 we show the core radius evolution with time for one of our best fit models. At its current age of 3.5 Myr the cluster is a little more than halfway to core collapse which will occur at ~ 4 Myr. This result is in agreement with the findings of Portegies Zwart et al. (2007).

6 SUMMARY

We have performed a large number of N -body simulations in order to find the best fitting model for the Arches cluster. The available observational data has been used to constrain the free parameters in our model. In a systematic analysis, we compared the total mass, the cumulative mass profile, and the present-day MF and defined fitness parameters for each of the three observables.

The main conclusion from our analysis is that the Arches cluster, despite of being born in an extreme environment, has formed with a standard Salpeter IMF. Due to mass segregation, the slope of the observed MF is flattened inside a radius of 0.4 pc. This radius was imposed a limit from the observational data used, and we estimate that a limiting radius of ~ 1 pc would be required for the observed MF to match the underlying IMF.

We conclude from our best fitting models that the Arches cluster was born with an initial virial radius of 0.76 ± 0.12 pc and an initial total mass of about $(5.1 \pm 0.8) \cdot 10^4 M_{\odot}$ assuming a lower mass limit of $0.5 M_{\odot}$ for the Salpeter IMF. The lower mass limit cannot be constrained well from our models, giving rise to additional uncertainties in determining the initial cluster mass. The King model concentration parameter of the best fitting models is $W_0 = 3 - 5$, however, the $W_0 = 7$ produced also reasonable fits so that this parameter is not very well constrained.

We neglected the Galactic potential and also stellar evolution for the simulations in this paper. These processes will be included in a following paper to get a more realistic model of the Arches cluster, however this first step was needed in order to reduce the number of free parameters for the these (computationally more expensive) simulations, which further constrain the dynamical evolution and tidal effects acting on the Arches cluster, and thereby the initial conditions of this nearby starburst, such as the cluster mass, the orbital motion and the IMF at the birth of the cluster.

Acknowledgments SH and SPZ are grateful for the support from the NWO Computational Science STARE project #643.200.503 and NWO grant #639.073.803. AS acknowledges funding from the German Science Foundation (DFG) Emmy-Noether-Programme under grant STO 496-3/1.

REFERENCES

- Casertano S., Hut P., 1985, *ApJ*, 298, 80
 Espinoza P., Selman F. J., Melnick J., 2009, *A&A*, 501, 563
 Figer D. F., Kim S. S., Morris M., Serabyn E., Rich R. M., McLean I. S., 1999, *ApJ*, 525, 750
 Figer D. F., Najarro F., Gilmore D., Morris M., Kim S. S., Serabyn E., McLean I. S., Gilbert A. M., Graham J. R., Larkin J. E., Levenson N. A., Teplitz H. I., 2002, *ApJ*, 581, 258
 Gaburov E., Harfst S., Portegies Zwart S., 2009, *New Astronomy*, 14, 630
 Heggie D. C., Mathieu R. D., 1986, in P. Hut & S. L. W. McMillan ed., *The Use of Supercomputers in Stellar Dynamics* Vol. 267 of *Lecture Notes in Physics*, Berlin Springer Verlag, Standardised Units and Time Scales. p. 233
 Kim S. S., Figer D. F., Kudritzki R. P., Najarro F., 2006, *ApJ*, 653, L113
 Kim S. S., Figer D. F., Lee H. M., Morris M., 2000, *ApJ*, 545, 301
 Kim S. S., Morris M., Lee H. M., 1999, *ApJ*, 525, 228
 King I. R., 1966, *AJ*, 71, 64
 Kroupa P., 2002, *Science*, 295, 82
 Lejeune T., Schaerer D., 2001, *A&A*, 366, 538
 Najarro F., Figer D. F., Hillier D. J., Kudritzki R. P., 2004, *ApJ*, 611, L105
 Portegies Zwart S., Gaburov E., Chen H.-C., Gürkan M. A., 2007, *MNRAS*, 378, L29
 Portegies Zwart S. F., Makino J., McMillan S. L. W., Hut P., 2002, *ApJ*, 565, 265
 Portegies Zwart S. F., McMillan S. L. W., Hut P., Makino J., 2001, *MNRAS*, 321, 199
 Press W. H., Teukolsky S. A., Vetterling W. T., Flannery B. P., 1992, *Numerical recipes in FORTRAN. The art of scientific computing*
 Salpeter E. E., 1955, *ApJ*, 121, 161
 Stolte A., 2003, PhD thesis, Combined Faculties for the Natural Sciences and for Mathematics of the Ruperto-Carola University of Heidelberg, Germany for the degree of Doctor of Natural Sciences. III
 Stolte A., Brandner W., Grebel E. K., Lenzen R., Lagrange A.-M., 2005, *ApJ*, 628, L113
 Stolte A., Ghez A. M., Morris M., Lu J. R., Brandner W., Matthews K., 2008, *ApJ*, 675, 1278
 Stolte A., Grebel E. K., Brandner W., Figer D. F., 2002, *A&A*, 394, 459